Journal of Applied Physics

Tunable magnetoelastic anisotropy in epitaxial (111) $Tm_3Fe_5O_{12}$ thin films EP

Cite as: J. Appl. Phys. **127**, 153905 (2020); https://doi.org/10.1063/1.5142856
Submitted: 18 December 2019 . Accepted: 28 March 2020 . Published Online: 21 April 2020

Nguyen M. Vu, Peter B. Meisenheimer, and John T. Heron

Journal of Applied Physics
ARTICLE
scitation.org/journal/jap

Tunable magnetoelastic anisotropy in epitaxial (111) $Tm_3Fe_5O_{12}$ thin films

Cite as: J. Appl. Phys. **127**, 153905 (2020); doi: 10.1063/1.5142856
Submitted: 18 December 2019 · Accepted: 28 March 2020 ·

Nguyen M. Vu, Peter B. Meisenheimer, and John T. Heron[a)]

AFFILIATIONS

Department of Materials Science and Engineering, University of Michigan, Ann Arbor, Michigan 48109, USA

[a)]**Author to whom correspondence should be addressed:** jtheron@umich.edu

ABSTRACT

Ferrimagnetic insulators with perpendicular magnetic anisotropy are of particular interest for spintronics due to their ability to mitigate current shunting in spin–orbit torque heterostructures and enable low switching energy, high-density storage magnetic devices. Rare earth iron garnet $Tm_3Fe_5O_{12}$ (TmIG) is one such material where prior studies have shown that the negative magnetostriction coefficient and isotropic in-plane tensile strain enable the magnetoelastic anisotropy to overcome the demagnetization energy and stabilize perpendicular magnetic anisotropy. However, the investigation of the tunability of the magnetoelastic anisotropy between thin films that possess perpendicular magnetization and quantification of the magnetoelastic constants has not been reported. Here, we quantify the evolution of magnetic anisotropy in (111)-oriented, epitaxial, 17 nm thick thin films of TmIG using a systematic variation of in-plane epitaxial strain (ranging 0.49%–1.83%) imposed by a suite of commercially available garnet substrates. Within the confines of the imposed strain range and deposition condition, the distortion from cubic symmetry is found to be approximately linear within the in-plane strain. The magnetic anisotropy field can be tuned by a factor of 14 in this strain range. The magnetoelastic anisotropy constant, B_2, is found to be approximately constant ($\sim$2500 kJ m^{-3}) and more than 2× larger than the reported bulk value ($\sim$1200 kJ m^{-3}) for a cubic distortion between 90.17° and 90.71°. B_2 is found to decrease at cubic distortions of 90.74° and larger. Our results highlight strain engineering, and its limitations, for control of perpendicular magnetic anisotropy.

I. INTRODUCTION

The projected end of Moore's law has spurred a tremendous effort into the discovery of new magnetic materials and heterostructures to advance logic and logic-in-memory devices.[1–3] Such magnetic technologies require reliable switching and low switching energy to replace high-power consumption transistors in modern electronic devices. New material systems, for instance, multiferroic and magnetoelectric heterostructures or spin–orbit torques from heavy metal/topological insulators, have been studied intensively, and yet still display major drawbacks such as low endurance, low detection signal, or high current shunting.[4–8] Recently, ferrimagnetic insulators (FIs)[9] have generated interest due to the realization of high quality thin films with perpendicular magnetization using a variety of fabrication techniques.[10–13] This development has led to the demonstration of efficient current-induced control of magnetization,[14–16] current-driven domain wall motion,[17] and high temperature quantum anomalous Hall effect in FI/topological insulator heterostructures.[18] Unlike conducting ferromagnets through which both charge and spin current can propagate, only spin current can pump through the surface of FIs to generate spin torque for modulating the magnetization,[16] which significantly reduces heat dissipation as well as writing current. Furthermore, overcoming the demagnetizing field in FIs that exhibit perpendicular magnetic anisotropy drives the switching current threshold lower when compared to a magnet with in-plane anisotropy.[19–21] For a magnetic with perpendicular magnetic anisotropy in a spin–orbit torque heterostructure, the critical current expression $J_c = \frac{\alpha}{\eta}\frac{2e}{\hbar} t H_K M_s$[19] emphasizes the need to reduce the anisotropy field H_K for switching efficiency. When approaching nanoscale dimensions and the mono-domain limit for device miniaturization, however, thermal fluctuation can cause instability, which can only be overcome by increasing the anisotropy field. Thus, there is a need to understand and quantify the evolution of H_K in FIs with perpendicular magnetic anisotropy so that optimized conditions can be engineered for future devices at scale. Previous studies have demonstrated the change in thin film anisotropy from in-plane to out-of-plane using strain[10,22] or tuning of perpendicular anisotropy field by changing film composition and therefore changing tensile strain.[12] The use of strain independently for anisotropy field tuning between thin films that possess perpendicular magnetization has not been reported nor thin film magnetoelastic coefficients been quantified.

Bulk ferrimagnetic TmIG crystallizes in a cubic crystal structure with a lattice constant of approximately 12.32 Å. Prior work[10–15] has shown that TmIG can be grown epitaxially on (111)-oriented GGG substrates and have a strain-induced perpendicular magnetic anisotropy described by Eq. (1) (see the supplementary material),

$$\Delta K_u = -\frac{K_1}{12} - \frac{1}{2}\mu_o M_s^2 + \frac{9}{4}\lambda_{111} c_{44}\left(\frac{\pi}{2} - \beta\right) \tag{1}$$

or

$$\Delta K_u = -\frac{K_1}{12} - \frac{1}{2}\mu_o M_s^2 - \frac{3}{4} B_2\left(\frac{\pi}{2} - \beta\right), \tag{2}$$

where K_1 is the cubic anisotropy constant, B_2 is the magnetoelastic coefficient, M_s is saturation magnetization, and β is the shear distortion angle from cubic symmetry (Fig. 1). Here, $B_2 = -3\lambda_{111} c_{44}$ where λ_{111} is the magnetostriction coefficient and c_{44} is the shear stiffness constant. In bulk, $K_1 = -0.58\,\text{kJ m}^{-3}$, $\lambda_{111} = -5.2 \times 10^{-6}$, $c_{44} = 76.6$ GPa, and $M_s = 110\,\text{emu cm}^{-3}$.[9,15] K_1 and λ_{111} being negative reveals that the distortion angle in a film must be larger than $\frac{\pi}{2}$ (e.g., from an isotropic in-plane tensile strain) to overcome shape anisotropy and achieve an out-of-plane easy axis.

In this work, we report the systematic tuning of magnetic anisotropy of (111)-oriented TmIG thin films using epitaxial strain imposed from a suite of commercially available rare earth garnet substrates that includes $Gd_3Ga_5O_{12}$ (GGG), $Y_3Sc_2Ga_3O_5$ (YSGG), $Gd_{2.6}Ca_{0.4}Ga_{4.1}Mg_{0.25}Zr_{0.65}O_{12}$ (SGGG), $Nd_3Ga_5O_{12}$ (NGG), and $Gd_3Sc_2Ga_3O_{12}$ (GSGG). The strain tuning of the magnetic anisotropy field by a factor of 14 in the considered strain range is shown. The magnetoelastic anisotropy constant, B_2, is found to be approximately $2500\,\text{kJ m}^{-3}$, more than 2× larger than the reported bulk value, for moderate cubic distortions and found to decrease sharply at cubic distortions of 90.74° and larger. The results demonstrate strain tuning as a pathway to design magnetic anisotropy in insulating ferrimagnets for device scaling purposes and future integrated heterostructures.

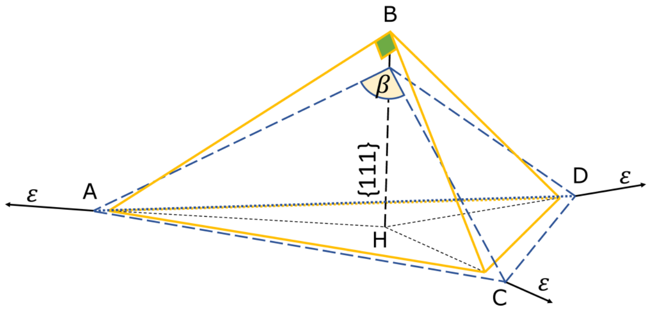

FIG. 1. Schematic showing the lattice distortion of (111)-oriented TmIG thin films on (111)-oriented garnet substrates. β is the distortion angle and black arrows represent the directions of resultant in-plane strain that increases β. The undistorted [111]-oriented cubic structure is shown with the solid orange lines for reference.

II. MATERIALS AND METHODS

(111)-oriented single crystal TmIG films were fabricated using pulsed laser deposition by ablating a stoichiometric $Tm_3Fe_5O_{12}$ target from PVD products with a 248 nm KrF excimer laser with a pulse duration of ∼25 ns. Commercially available (111)-oriented single crystal 0.5 mm thick GGG, YSGG, SGGG, NGG, and GSGG from MTI Corporation were used to systematically tune the epitaxial strain. The substrates provide an ideal in-plane tensile strain spanning 0.485%–1.83% with distortion angle nominal values ranging from 90.22° to 90.93°, which were determined based on the database from the manufacturer and Poisson's ratio of TmIG $\upsilon = 0.3$.[8] (Table S1 in the supplementary material). Film growth was carried out at a temperature of 850 °C, a fluence of $1.2\,\text{J cm}^{-2}$, a laser repetition frequency of 6 Hz, and an O_2 background pressure of 180 mTorr. These conditions were found to maintain relatively uniform crystallinity and out-of-plane magnetic anisotropy among all films. All substrates ($\sim 2.5 \times 2.5\,\text{mm}^2$ in size) were deposited on simultaneously to keep process conditions constant between samples. Thereby the nominal difference between films is the imposed strain from each individual substrate. Structural characterization of TmIG thin films in the form of $2\theta - \omega$ x-ray diffraction, x-ray reflectivity, and reciprocal space mapping was performed using a Rigaku Smartlab diffractometer with CuK_α radiation. The film thicknesses were determined from x-ray reflectivity and were nominally 17 nm (Table S2 and Fig. S1 in the supplementary material). Magnetic characterization was performed at room temperature using a Lakeshore vibrating sample magnetometer in order to assess the evolution of magnetization and magnetic anisotropy. The paramagnetic signal from the underlying substrate was removed from the reported loops by subtraction of the high field slope in moment vs magnetic field scans. Hysteresis loops were fit to the Stoner–Wohlfarth macrospin model using the native curve_fit function in Python3. Anisotropy energy values extracted from the fits themselves agree with the empirically measured anisotropy fields within the covariance of the fits.

III. RESULTS AND DISCUSSION

A. Structural characterization

X-ray diffraction was used to assess the epitaxy, crystallinity, and strain state of the TmIG films. X-ray symmetric scans around the 444 diffraction peaks of the 17 nm TmIG films are shown in Fig. 2(a). Intensity oscillations around film peaks indicate excellent crystallinity and smooth interfaces. The evolution of the film peak position with respect to the substrate peak position reveals an increasing out-of-plane compressive strain in agreement with the expected increasing in-plane tensile strain from the substrate. To confirm the epitaxial growth of TmIG on each substrate, reciprocal space maps (RSMs) around the 624 peaks were performed [Fig. 2(b)]. RSMs of TmIG films on GGG, YSGG, SGGG, and NGG

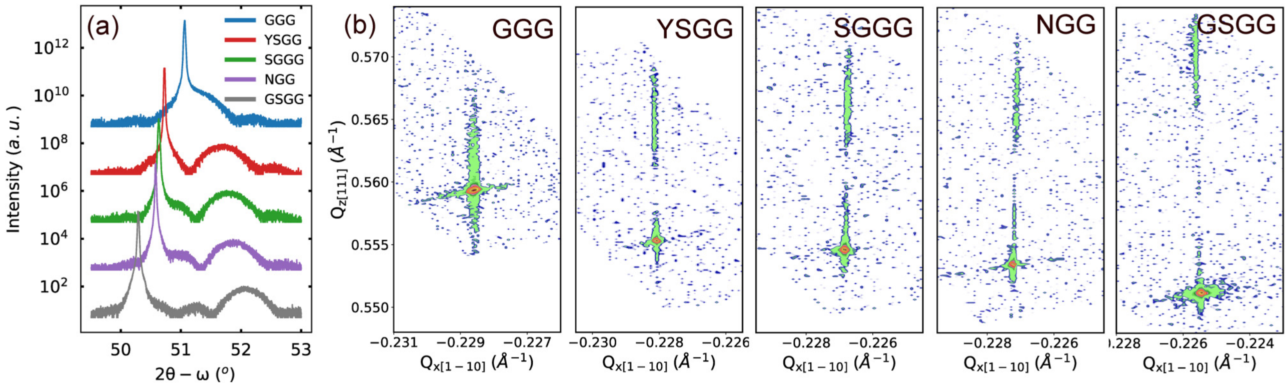

FIG. 2. Structural characterization and coherent strain tuning of 17 nm thick TmIG thin films on garnet substrates. (a) Symmetric $2\theta - \omega$ scan around the 444 diffraction peaks of the film and substrate. Data have been vertically offset for clarity. The out-of-plane lattice parameter of the TmIG films systematically decreases with increasing substrate lattice parameter and is pseudomorphic to the substrate. (b) Reciprocal space map of asymmetric scan around 624 peaks of TmIG films (upper peaks) on GGG, YSGG, SGGG, NGG, and GSGG substrates, respectively.

show that the films are fully strained with the same in-plane lattice constants as their associated substrates. TmIG grown on GSGG experiences a small relaxation through a slight shift of the film peak with respect to the substrate ($\Delta Q_x = 1.6 \times 10^{-4}$ Å^{-1} $\leftrightarrow \Delta a = 9 \times 10^{-3}$ Å, Q_x step size is 6.56×10^{-5} Å^{-1}). The evolution of out-of-plane lattice parameters of TmIG films observed in RSM scans also relatively agree with that observed in symmetric x-ray scans (Table I). In order to determine anisotropy energy [Eq. (1)], the distortion angle, β, is then evaluated.

The distortion angle can be calculated from RSM scans using the assumption that in-plane strain will result in a change in the d_{111} spacing and distorting cubic edges (BA, BC, and BD in Fig. 1).

TABLE I. Lattice constants of substrates and films correspondingly from x-ray diffraction (units in Angstroms).

Substrate	a_{sub} (Q_x)[a]	a_{sub} (Q_z)[b]	a_{sub} $(2\theta\text{–}\omega)$[c]	a_{film} (Q_z)[d]	a_{film} $(2\theta\text{–}\omega)$[e]	β
GGG	12.37	12.39	12.38	12.32	12.31	90.17
YSGG	12.40	12.48	12.46	12.25	12.24	90.47
SGGG	12.47	12.49	12.48	12.22	12.22	90.74
NGG	12.45	12.52	12.49	12.22	12.20	90.71
GSGG	12.54	12.57	12.56	12.16	12.15	91.17

[a] a_{sub} (Q_x) (in-plane lattice parameter of the substrate) determined from the RSM Q_x value of each substrate.

[b] a_{sub} (Q_z) (out-of-plane lattice parameter of the substrate) determined from the RSM Q_z value of each substrate.

[c] a_{sub} $(2\theta\text{–}\omega)$ (out-of-plane lattice parameter of the substrate) determined from d_{444} spacing of substrate peak from $2\theta\text{–}\omega$ scan.

[d] a_{film} (Q_z) (out-of-plane lattice parameter of the thin film) determined from the RSM Q_z value of each film.

[e] a_{film} $(2\theta\text{–}\omega)$ (out-of-plane lattice parameter of the thin film) determined from d_{444} spacing of film peak from $2\theta\text{–}\omega$ scan.

The distortion angle β is then determined by

$$\cos\beta = \frac{2BC^2 - AC^2}{2BC^2}, \tag{3}$$

where $AC = a\sqrt{2}$ and $BC = \left[\left(\frac{d_{111}}{3}\right)^2 + \frac{2a^2}{3}\right]^{\frac{1}{2}}$, a is the cubic lattice constant of substrate and d_{111} is out-of-plane spacing (diagonal of the cube), which are both obtained from RSM data [a_{sub} (Q_x) and a_{film} (Q_z)]. Table I shows lattice constants of substrates and films calculated from x-ray diffraction measurements. The distortion angles are found to be greater than 90° revealing the in-plane (out-of-plane) tensile (compressive) strain that generally increases with increasing in-plane strain and demonstrates the control of the biaxial strain state in TmIG thin films. With the distortion angle calculated, magnetic measurements allow us to then quantify the evolution of the magnetic anisotropy.

B. Tuning of magnetic anisotropy

Room temperature magnetic hysteresis measurements were run on all samples with the magnetic field in-the-plane and out-of-the-plane of the film surface to determine the saturation magnetization, magnetic anisotropy direction, and anisotropy field. All films possess an out-of-plane easy axis with comparable saturation magnetization excepting the film grown on GSGG. Figure 3(b) shows out-of-plane hysteresis loops for all TmIG films. The saturation magnetization vs distortion angle is shown in Fig. 3(c). The saturation magnetization is approximately constant (~90 emu cm^{-3}) for distortion angles at and below 90.74° with a sudden drop in magnetization for the film on GSGG ($\beta = 91.17°$). While unclear, this drop in magnetization may be correlated with the slight relaxation observed from RSM results as well as topographic features that are unique to this film (Fig. S2 in the supplementary material).

For a sample with perpendicular magnetic anisotropy, the anisotropy field is the field needed for the magnetization to

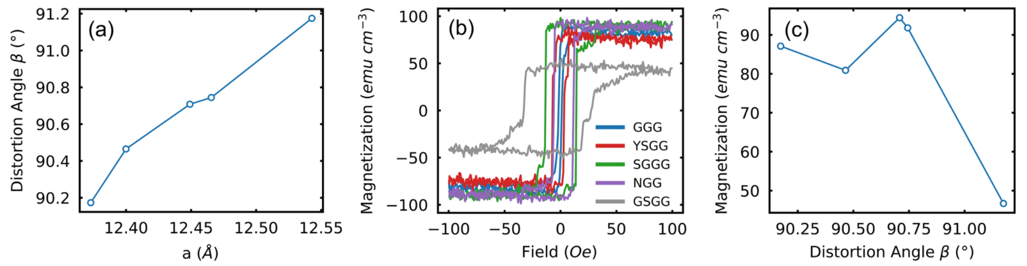

FIG. 3. Magnetic characterization. (a) Distortion angle of the TmIG films on the different garnet substrates, as a function of cubic lattice parameter that was obtained from RSM Q_x scans shown in Fig. 2. The distortion angle from cubic symmetry increases approximately linearly with the increasing in-plane substrate lattice parameter. (b) Room temperature out-of-plane magnetization vs magnetic field loops of 17 nm thick TmIG thin films on different substrates. The TmIG thin films show clear perpendicular magnetic anisotropy. (c) Saturation magnetization vs distortion angle β. The saturation magnetization is approximately constant (∼90 emu cm^{-3}) for distortion angles at and below 90.74° but drops significantly for the film on GSGG ($\beta = 91.17°$).

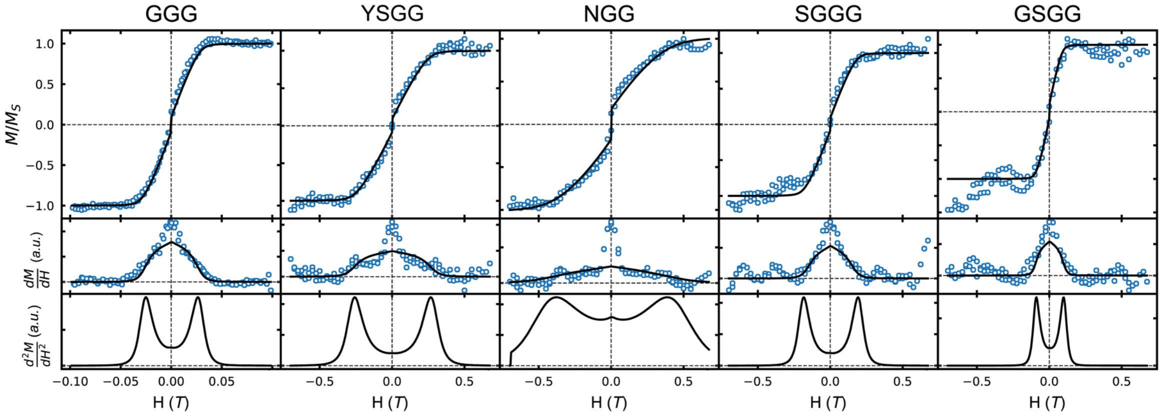

FIG. 4. Measurement of anisotropy energies. Top row: Room temperature, in-plane magnetization vs magnetic field loops of 17 nm thick TmIG thin films on different substrates. Data are shown as open circles, and fits to the Stoner–Wohlfarth macrospin model are shown as a black line. The curvature of the hysteresis loops is from an ∼5° offset from the in-plane hard axis due to experimental setup. Middle row: First derivative of normalized in-plane loops (points), shown with the first derivative of the calculated fits in black. Bottom row: Second derivative of magnetometry fits. Anisotropy fields are extracted using the peaks of the second derivative with a field resolution of 1 Oe.

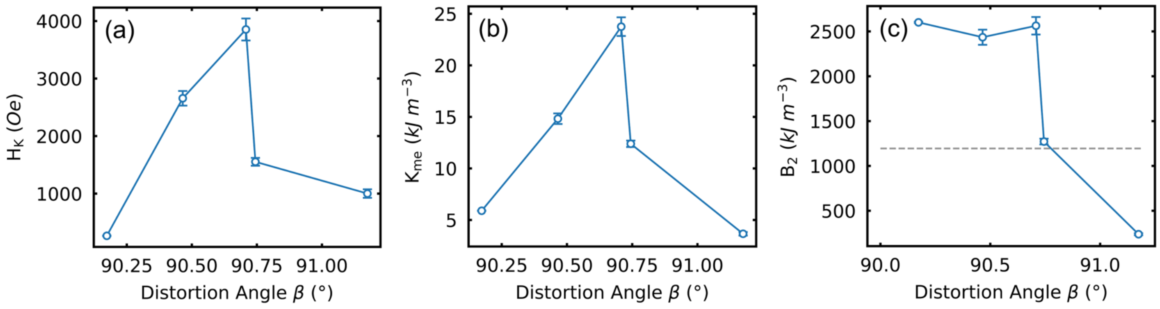

FIG. 5. Tuning of magnetic anisotropy with epitaxial strain. (a) Anisotropy field, (b) magnetoelastic anisotropy energy, and (c) magnetoelastic coupling constant (B_2) as a function of film distortion angle β. The magnitude of the anisotropy field and magnetoelastic anisotropy energy generally increases with increasing strain up to a distortion angle of ∼90.71°, after which a decrease with increasing distortion angle is observed. The anisotropy field can be tuned up to a factor of ∼14 in the distortion angle range of 90.17°–90.71°. The magnetoelastic anisotropy constant is ∼2 times larger than the bulk value for some strains. The dashed horizontal line in (c) indicates the bulk value.

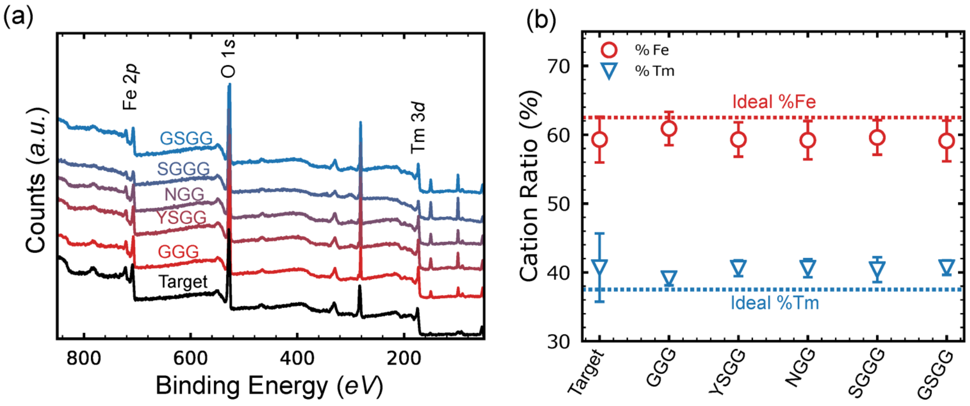

FIG. 6. X-ray photoelectron spectroscopy data from TmIG target and films on various substrates. The XPS data show that the composition of the films and the target are the same within the error of the analysis. Error bars were calculated from the standard deviation of the composition based on the energy analysis window. The uniform Fe deficiency among all films supports our conclusion that the differences between magnetoelastic constants are coming from the strain from substrates.

overcome the energy barrier between in-plane and out-of-plane states.[23,24] In this work, anisotropy fields are determined by measuring in-plane magnetic field strength that saturates the magnetization and quantitatively extracted from the second derivative of the in-plane loops[25] (Fig. 4). Figure 5(a) shows the magnetic anisotropy field vs distortion angle, β. This tuning window is defined by strain independently at our specific deposition condition and does not consider tuning from different growth parameters such as oxygen background pressure. The anisotropy tends to increase with increasing distortion angle with the exception of GSGG and SGGG. To further access this trend in the anisotropy field, magnetoelastic contributions are calculated next. Since the values of shear stiffness for thin films are unknown (and thusly for magnetostriction), we report here the value of magnetoelastic constants $B_2 = -3\lambda_{111}c_{44}$ for our TmIG thin films in each substrate reflecting the relationship between lattice deformation and its magnetization.[26] We see that B_2 stays relatively constant for the thin film at low strains (but is ~2 times larger than bulk) until β reaches ~90.74° [Fig. 5(c)]. The small B_2 values in these thin films justify their small anisotropy fields despite the contribution from large lattice distortion. The thin film magnetoelastic coefficient may differ from bulk for several reasons: unlike bulk, the film is clamped to a substrate so it is not free to deform in-plane but free to deform out-of-plane, surface magnetostriction, and other surface effects (structural and chemical defects) may become significant at these film thicknesses, and compositional variance. The enhanced B_2 in films may be a result of one or more of the above factors. To shed some light on the evolution of the magnetic properties, x-ray photoelectron spectroscopy was performed on the TmIG target and films on various substrates. The XPS data show that the composition of the films and the target are the same within the error of the analysis, yet there is a uniform Fe deficiency among all (Fig. 6). Thus, the evolution of anisotropy field, anisotropy energy, and magnetoelastic constant between films is a result of the strain from substrates.

IV. CONCLUSION

In summary, we have investigated the modulation of magnetic anisotropy of rare earth garnet TmIG (111)-oriented single crystal thin films subjected to different isotropic in-plane tensile strains. Overall, the magnitude of the magnetoelastic anisotropy energy increases with increasing strain, with the exception of the thin film grown on GSGG where a significant decrease in saturation magnetization, anisotropy field, and magnetoelastic anisotropy constant is observed. The magnitude of the anisotropy field can be increased up to a factor of 14, with a maximal anisotropy field of ~3900 Oe, within our studied strain range and deposition condition. Such tunability provides a knob to engineer the performance and scalability of magnetic devices that employ TmIG. Finally, we find that the magnetoelastic anisotropy constant B_2 is approximately more than 2× larger than in bulk at low strains.

SUPPLEMENTARY MATERIAL

See supplementary material for the derivation of the magnetoelastic anisotropy, x-ray reflectometry, and atomic force microscopy.

ACKNOWLEDGMENTS

This work was supported by the Semiconductor Research Corporation (SRC) at the NEWLIMITS Center and NIST through Award Number 70NANB17H041. This work was partially supported by NSF CAREER Grant No. DMR-1847847.

REFERENCES

[1] S. Manipatruni, D. E. Nikonov, C.-C. Lin, T. A. Gosavi, H. Liu, B. Prasad, Y.-L. Huang, E. Bonturim, R. Ramesh, and I. A. Young, Nature **565**, 35 (2019).
[2] N. A. Spaldin and R. Ramesh, Nat. Mater. **18**, 203 (2019).
[3] P. B. Meisenheimer, S. Novakov, N. M. Vu, and J. T. Heron, J. Appl. Phys. **123**, 240901 (2018).
[4] J. T. Heron, J. L. Bosse, Q. He, Y. Gao, M. Trassin, L. Ye, J. D. Clarkson, C. Wang, J. Liu, S. Salahuddin, D. C. Ralph, D. G. Schlom, J. Íñiguez, B. D. Huey, and R. Ramesh, Nature **516**, 370 (2014).

[5]X. He, W. Echtenkamp, and Ch. Binek, Ferroelectrics **426**, 81 (2012).
[6]N. H. D. Khang, Y. Ueda, and P. N. Hai, Nat. Mater. **17**, 808 (2018).
[7]T. Kosub, M. Kopte, R. Hühne, P. Appel, B. Shields, P. Maletinsky, R. Hübner, M. O. Liedke, J. Fassbender, O. G. Schmidt, and D. Makarov, Nat. Commun. **8**, 13985 (2017).
[8]M. Dc, R. Grassi, J.-Y. Chen, M. Jamali, D. Reifsnyder Hickey, D. Zhang, Z. Zhao, H. Li, P. Quarterman, Y. Lv, M. Li, A. Manchon, K. A. Mkhoyan, T. Low, and J.-P. Wang, Nat. Mater. **17**, 800 (2018).
[9]A. Paoletti, in *Physics of Magnetic Garnets* (Italian Physical Society, 1978).
[10]M. Kubota, K. Shibuya, Y. Tokunaga, F. Kagawa, A. Tsukazaki, Y. Tokura, and M. Kawasaki, J. Magn. Magn. Mater. **339**, 63 (2013).
[11]M. Kubota, A. Tsukazaki, F. Kagawa, K. Shibuya, Y. Tokunaga, M. Kawasaki, and Y. Tokura, Appl. Phys. Express **5**, 103002 (2012).
[12]C. N. Wu, C. C. Tseng, Y. T. Fanchiang, C. K. Cheng, K. Y. Lin, S. L. Yeh, S. R. Yang, C. T. Wu, T. Liu, M. Wu, M. Hong, and J. Kwo, Sci. Rep. **8**, 11087 (2018).
[13]C. N. Wu, C. C. Tseng, K. Y. Lin, C. K. Cheng, S. L. Yeh, Y. T. Fanchiang, M. Hong, and J. Kwo, AIP Adv. **8**, 055904 (2018).
[14]C. O. Avci, A. Quindeau, C.-F. Pai, M. Mann, L. Caretta, A. S. Tang, M. C. Onbasli, C. A. Ross, and G. S. D. Beach, Nat. Mater. **16**, 309 (2017).
[15]A. Quindeau, C. O. Avci, W. Liu, C. Sun, M. Mann, A. S. Tang, M. C. Onbasli, D. Bono, P. M. Voyles, Y. Xu, J. Robinson, G. S. D. Beach, and C. A. Ross, Adv. Electron. Mater. **3**, 1600376 (2017).
[16]P. Li, J. Kally, S. S.-L. Zhang, T. Pillsbury, J. Ding, G. Csaba, J. Ding, J. S. Jiang, Y. Liu, R. Sinclair, C. Bi, A. DeMann, G. Rimal, W. Zhang, S. B. Field, J. Tang, W. Wang, O. G. Heinonen, V. Novosad, A. Hoffmann, N. Samarth, and M. Wu, Sci. Adv. **5**, eaaw3415 (2019).
[17]S. Vélez, J. Schaab, M. S. Wörnle, M. Müller, E. Gradauskaite, P. Welter, C. Gutgsell, C. Nistor, C. L. Degen, M. Trassin, M. Fiebig, and P. Gambardella, Nat. Commun. **10**, 4750 (2019).
[18]C. Tang, Y. Liu, Z. Jiang, J. Shi, C.-Z. Chang, J. S. Moodera, C.-X. Liu, G. Zhao, M. R. McCartney, D. J. Smith, and T. Chen, Sci. Adv. **3**, e1700307 (2017).
[19]J. Z. Sun, Phys. Rev. B **62**, 570 (2000).
[20]T. Taniguchi, S. Mitani, and M. Hayashi, Phys. Rev. B **92**, 024428 (2015).
[21]L. Liu, C.-F. Pai, Y. Li, H. W. Tseng, D. C. Ralph, and R. A. Buhrman, Science **336**, 555 (2012).
[22]G. Li, H. Bai, J. Su, Z. Z. Zhu, Y. Zhang, and J. W. Cai, APL Mater. **7**, 041104 (2019).
[23]D. H. Kim, N. M. Aimon, L. Bi, J. M. Florez, G. F. Dionne, and C. A. Ross, J. Phys. Condens. Matter **25**, 026002 (2013).
[24]J.-M. Hu and C. W. Nan, Phys. Rev. B **80**, 224416 (2009).
[25]G. Turilli, J. Magn. Magn. Mater. **130**, 377 (1994).
[26]V. Z. C. Paes and D. H. Mosca, J. Magn. Magn. Mater. **330**, 81 (2013).